Passive mode-locking and terahertz frequency comb generation in resonant-tunneling-diode oscillator

Tomoki Hiraoka
Kyoto University https://orcid.org/0000-0002-3199-6264
Yuta Inose
Kyoto University
Takashi Arikawa
Kyoto university https://orcid.org/0000-0002-7330-2275
Hiroshi Ito
Kitasato University
Koichiro Tanaka (kochan@scphys.kyoto-u.ac.jp)
Kyoto University https://orcid.org/0000-0002-2132-8318

Article

Keywords: Optical frequency combs, terahertz frequency range, optical feedback, terahertz sensing

Posted Date: November 9th, 2021

DOI: https://doi.org/10.21203/rs.3.rs-919266/v1

Version of Record: A version of this preprint was published at Nature Communications on June 29th, 2022. See the published version at https://doi.org/10.1038/s41467-022-31071-3.

Title Passive mode-locking and terahertz frequency comb generation in resonant-tunneling-diode oscillator

Names Tomoki Hiraoka[1]*, Yuta Inose[1]*, Takashi Arikawa[1], Hiroshi Ito[2],

and Koichiro Tanaka[1]* (* corresponding author)

Affiliations

[1] Department of Physics, Graduate School of Science, Kyoto University, Sakyo-ku, Kyoto 606-8502, Japan

[2] Center for Natural Sciences, Kitasato University, Minami-ku, Sagamihara 252-0373, Japan

Contact information

Tomoki Hiraoka: hiraoka.tomoki.5z@kyoto-u.ac.jp

Yuta Inose: inose.yuta.3r@kyoto-u.ac.jp

Koichiro Tanaka: kochan@scphys.kyoto-u.ac.jp

Abstract

Optical frequency combs in the terahertz frequency range are long-awaited frequency standards for spectroscopy of molecules and high-speed communications. However, a terahertz frequency comb based on a compact, efficient and room-temperature-operating device remains unavailable especially in the frequency range of 0.1 to 3 THz. In this paper, we show that the resonant-tunneling-diode oscillator can be passively mode-locked by optical feedback and generate a terahertz frequency comb. The standard deviation of the spacing between the comb lines, i.e., the repetition frequency, is reduced to less than 420 mHz by applying external bias modulation. A simulation model successfully reproduces the mode-locking behavior by including the nonlinear capacitance of RTD and multiple optical feedback. Since the mode-locked RTD oscillator is a simple semiconductor device that operates at room temperature and covers the frequency range of 0.1 to 3 THz, it can be used as a frequency standard for future terahertz sensing and communications.

(Main text)

Introduction

The optical frequency comb is a crucial light source for metrology and spectroscopy. Its spectrum consists of equidistant optical modes [1]. The frequency of each mode is represented as follows:

$$f_n = f_{\mathrm{CEO}} + n f_{\mathrm{rep}}. \tag{1}$$

Here, f_{rep}, f_{CEO}, and n are the repetition frequency, carrier-envelope-offset frequency, and modal index, respectively. The optical modes are coherent and have a stable phase relationship with each other. The frequency-comb source is long-awaited as the frequency standard for spectroscopy of gaseous molecules [2] and high-speed communications in the terahertz frequency range [3]. However, such light sources typically depend on bulky, energy-consuming, and expensive femtosecond lasers [4]. Development of a compact, efficient and low-priced terahertz frequency-comb source based on a semiconductor device is still being pursued.

A promising candidate for a semiconductor-based terahertz frequency-comb source is the quantum cascade laser (QCL) [5], which is a compact device emitting watt-class terahertz waves [6][7]. A frequency comb using a terahertz QCL was recently demonstrated [8][9][10][11]. Moreover, differential frequency generation in mid-infrared QCL comb has been used to make a comb from 1.8 to 3.3 THz at room temperature [12][13]. However, it is difficult for a QCL to generate terahertz comb below 1.8 THz. There are also devices based on Si CMOS technologies. For instance, a frequency-comb source based on a multiplier was demonstrated for spectroscopy in the range from 220 to 330 GHz [14]. Moreover, a bipolar CMOS device was used to generate a frequency comb from 0.03 to 1.1 THz [15]. However, it is difficult for CMOS devices to generate terahertz waves of higher frequency.

This study reports a novel terahertz comb source, a passive mode-locked resonant-tunneling-diode (RTD) oscillator. The RTD oscillator is an electrical device with fundamental oscillation frequency in the terahertz frequency range at room temperature [16]. Oscillation from the sub-terahertz to 1.98 THz range has been achieved [17][18][19][20][21], and oscillation up to 2.77 THz is expected [22]. A single oscillator can be fabricated on a millimeter-sized chip [23]. The emission power reached 0.4 mW for a single oscillator at 530-590 GHz [24] and 0.73 mW for a large-scale array at 1 THz [25]. The DC-to-RF conversion efficiency in the terahertz region is about 1 % [24]. However, there has been no report on mode-locking and frequency comb generation in an RTD oscillator. In this paper, we show that the RTD oscillator can be passively mode-locked by simply controlling the optical feedback and that a terahertz frequency comb can be generated. We also demonstrate that the repetition frequency can be stabilized by external modulation. We present a simulation model which reproduces the mode-locking, and predict the future improvement in comb performance.

Results

Measurement of emission spectrum

Figure 1a is a schematic diagram of the experimental setup. We measured the emission spectrum of an RTD oscillator under optical feedback with variable amplitude and delay. The distance between the oscillator and the mirror z_{M} was about 500 mm. We performed a heterodyne measurement with the local oscillator (LO) signal, which had a center frequency of 303.5 GHz and a linewidth of less than 240 mHz at FHWM (see the Experimental setup section in the Methods.) Figure 1b shows a typical emission power spectrum of a continuous-wave (CW) oscillatory state observed without optical feedback from the mirror. It is a single-frequency spectrum with minor sidebands with much lower power spectral densities (PSD) compared with the main peak. The bottom axis shows the heterodyne frequency, and the top axis shows the corresponding terahertz frequency.

We found that a frequency comb is generated when optical feedback is injected into the RTD oscillator in a certain phase. The red trace in Figure 1c shows a typical frequency-comb spectrum. Including the small peaks that are not numbered in Figure 1c, there are optical modes with a mode spacing of 273.3 MHz. The mode spacing was approximately proportional to the inverse of z_{M}. This shows that optical feedback from the mirror causes the optical modes. We note that the mode spacing is not exactly equal to the free-spectral range of a Fabry-Perot cavity, i.e., $c/2z_{\mathrm{M}}$, where c is the speed of light. This is because the amplitude of the return light is small, and a good cavity is not formed in our setup, as described in Supplementary Section 8 (3-2). One in four optical modes has a large intensity. The RF frequencies of the numbered peaks are described with the following equation:

$$f_n^{\mathrm{RF}} = f_0^{\mathrm{RF}} + n f_{\mathrm{rep}}. \quad (2)$$

Here, f_n^{RF} is the RF frequency of the mode with index n, and f_0^{RF} is the offset RF frequency. We fitted the relationship between the frequencies of the comb lines f_n^{RF} (n = 0 to 9) and n with equation (2) and obtained the parameters with the average values and standard deviation as follows: $f_0^{\mathrm{RF}} = 618.97 \pm 0.45$ MHz and $f_{\mathrm{rep}} = 1093.13 \pm 0.11$ MHz (see the Spectrum characterization in the Methods). Since f_{rep} is an integer multiple of the mode spacing, it is a harmonic frequency comb [26][27]. In the present experiment, the harmonic frequency comb with a separation of 4 mode spacing was the most stable.

The peaks shown in the black trace of Figure 1c are homodyne signals that appeared even when we blocked the LO signal. Figure 1d shows the homodyne signal measured under the same conditions as those of Figure 1c. There are three peaks, and their frequencies match integer multiples of f_{rep} within the margin of error. Hence, the homodyne peaks are the inter-mode beat note of the harmonic comb. Figures 1e and 1f show the magnified spectrum of the comb line indexed as $n = 3$ and the homodyne peak at 1.0931 GHz. The linewidth of the comb line is 1.9 MHz. The homodyne peak has a smaller linewidth of 310 kHz. Its small linewidth corresponds to a small error in f_{rep} and implies that the optical modes are phase-locked to each other.

Relative modal phases

To clarify that the modal phases obey a stable relationship, we measured the single-shot temporal waveform of the heterodyne signal shown in Figure 1c. A sequential waveform was measured over 65.6 μs, as shown in Supplementary Section 2. The dots in Figure 2a show a typical part of the measured waveform, and the trace shows a fitting curve obtained in the analysis below. The heterodyne waveform has an average period of approximately 200 ps corresponding to the center RF frequency of 5 GHz in the comb spectrum. We can see that it has a frequency modulation with a period of approximately 1 ns. This frequency-modulated property is further clarified in the analysis below.

We performed a fitting analysis of the heterodyne waveform to clarify the phase relationship between the modes. We utilized a fitting function representing the heterodyne beat of the frequency comb:

$$f(t) = \sum_{n=2}^{6} A_n \sin\left[2\pi\left(f_0^{\mathrm{RF}} + n f_{\mathrm{rep}}\right)(t - t_0) + \varphi_n\right]. \quad (3)$$

Here, n is the modal index shown in Figure 1c. We considered only the five modes of n from 2 to 6, which have significant amplitudes. A_n denotes the amplitudes of the modes, which are fixed parameters derived from the spectrum. t_0 is the time origin. φ_n denote the initial phases at $t = t_0$. f_0^{RF}, f_{rep}, t_0, and φ_n are the fitting parameters. We neglected the phase fluctuation of the LO signal because its linewidth was less than 240 mHz.

We analyzed the long-term waveform of 65.6 μs to clarify the stability of the phase relationship. In the time scale defined by linewidths of the comb lines (1/1.9 MHz = 520 ns), noise causes a random phase shift in each mode. If the modes are not phase-locked, the phase relationship between the modes would be randomized in this time scale. When the modes are phase-locked, the modes keep a certain phase relationship, and the noise causes only a timing jitter of the mode-locked waveform. The waveform in 65.6 μs has random phase shift or timing jitter, so we cannot fit the entire waveform with equation (3), in which each frequency component is described as a single sinusoidal wave with a well-defined phase. We divided the long span of 65.6 μs into short spans of 164 ns and fitted the waveform in each short span. A typical fitting curve is shown as the trace in Figure 2a; it fits the data points. It is not a short and intense pulse, as is often the case for a mode-locked pulse. We note that we carefully defined the time origin t_0 in each short span to compensate the timing jitter and represent the relationship between the initial phases φ_n uniquely. We defined the time origin t_0 in each span as the time at which the condition $\varphi_3 = \varphi_4$ is satisfied. The details of the fitting are shown in Supplementary Section 3.

Figures 2b and 2c show f_0 and f_{rep} for each fitting span. The average values and standard deviations considering the fitting error are as follows: $f_0 = 618.039 \pm 0.061\ \mathrm{MHz}$ and $f_{\mathrm{rep}} = 1093.1500 \pm 0.0032\mathrm{MHz}$. The average values are consistent with those derived from the spectrum. The standard deviations are smaller than the linewidths in Figures 1e and 1f. It indicates that there is a long-term deviation not observed in this span. Figure 2d shows the *relative initial phase,* defined as $\Delta\varphi_n \equiv \varphi_n - \varphi_4$ in each fitting span. Surprisingly, they held the same relationship stably for 65.6 μs. Their average values and standard deviations are as follows: $\Delta\varphi_2 = -0.40 \pm 0.61$, $\Delta\varphi_5 = 3.29 \pm 0.48$, $\Delta\varphi_6 = 0.25 \pm 0.49$ rad. Their relation can be expressed approximately as

$$(\Delta\varphi_2, \Delta\varphi_3, \Delta\varphi_4, \Delta\varphi_5, \Delta\varphi_6) \cong (0,0,0,\pi,0). \quad (4)$$

This stable relationship between modal phases is clear evidence of mode-locking. We note that the relationship of equation (4) is different from that of the typical mode-locked lasers based on saturable absorbers. All the modes have the same phase in such lasers, and they show amplitude-modulated waveform. The relationship of equation (4) rather means a frequency-modulated waveform, as described in detail in Supplementary Section 4. Such a frequency-modulated waveform is also observed in the frequency comb generated in the QCL [28] and the mode-locked dark pulse generated in the microresonator [29].

Conditions for passive mode-locking

We found that passive mode-locking occurred only around a particular point in the frequency-voltage curve, which we call the "frequency jump." Figure 3a shows frequency-voltage curves measured over a wide range with and without optical feedback from the mirror. When there is no optical feedback, the curve shows a frequency jump of about 2 GHz around 471 mV. The frequency changes continuously at the other bias points. When feedback is present, many small steps appear in the frequency-voltage curves. The oscillation frequency shows a hysteretic behavior in the sweeping direction. A large hysteresis loop in the frequency-voltage curve formed at the frequency jump point of 471 mV. These behaviors can be qualitatively explained with the oscillation condition for a simplified circuit model with optical feedback [30], which is given in Supplementary Section 5. Furthermore, these frequency-voltage curves were reproduced in a simulation, as shown in the next section. When the bias voltage is set near the frequency jump point and the position of the mirror is swept, the passive mode-locking state appears. Figure 3b shows the detailed frequency-voltage curve measured near the frequency jump and the peak frequencies of the comb (green crosses). We swept the mirror at bias voltages from 467 to 475 mV in 0.5 mV steps and obtained the comb spectra only in the range of 470 to 472 mV, which is the vicinity of the frequency jump.

The comb spectra appeared at a particular mirror position. Figure 3c shows the heterodyne spectrum measured by sweeping the mirror in steps of 0.02 mm at a fixed voltage of 471 mV. The comb spectra were observed periodically to the mirror position, as shown by the vertical lines on the top of Figure 3c. The period was 0.500 mm. The round-trip length of 1.000 mm is equal to the wavelength of the terahertz wave of 300 GHz. This shows that passive mode-locking takes place at a certain phase of the optical feedback.

In the present experiment, the feedback amplitude was close to the lower limit of the passive mode-locking. When the feedback amplitude was reduced to less than 93 % of the maximum amplitude, the passive mode-locked state disappeared. The details of the feedback amplitude dependence are described in Supplementary Section 6.

Hybrid mode-locking

We succeeded in stabilizing the repetition frequency by using the hybrid mode-locking technique [31], in which an additional bias modulation is applied to the passively mode-locked oscillator. Figure 1g shows a magnified view of the spectrum of the inter-mode beat note in the hybrid mode-locked state. The modulation frequency was set to 1.0932 GHz (with a linewidth of less than 1 Hz), which is the same as the harmonic-comb spacing of the passive mode-locked state. By applying the modulation, the linewidth of the inter-mode beat note decreased to less than 1 Hz. It corresponds to the standard deviation of 420 mHz in the repetition frequency. The output power of the modulator was only -40 dBm, while the emission power from the RTD oscillator was -20 dBm. In the hybrid mode-locked state, the linewidth of the comb lines did not change from that of the passive mode-locked state. This means that the carrier-envelope-offset frequency of the comb lines was not stabilized by the hybrid mode-locking. Moreover, the amplitudes of the modes did not change. The details of the hybrid mode-locking and conditions for achieving hybrid mode-locking are described in Supplementary Section 7.

A circuit model for the passive-mode locking

Here, we present a circuit simulation model that reproduces the frequency-voltage curve, the frequency comb in the vicinity of the frequency jump, and the frequency-modulated waveform. The model simulates an LCR parallel circuit with an RTD. It includes not only the nonlinear conductance but also the nonlinear capacitance of the RTD [32][33][34]. The optical feedback is included as feedback current $I_{\mathrm{FB}} = \sqrt{\eta} I_{\mathrm{load}}(t - t_d)$. Here, $I_{\mathrm{load}}(t)$ is the current at the load in the circuit, and t_d is the time delay. η is a *reflectivity* including the coupling efficiency. Noise in the circuit is included. The circuit diagram and parameters are given in Supplementary Section 8 (1).

Figure 4a shows a simulated frequency-voltage curve that reproduces the experimentally measured curve in Figure 3a. To reproduce the frequency jump, we found that two additional optical-feedback terms with parameters (t_d, η) of (19.7 ps, $10^{-2.0}$) and (178 ps, $10^{-3.0}$) were necessary [see Supplementary Section 8 (3-1)]. They correspond to reflection surfaces separated from the oscillator by 2.95 mm and 26.7 mm, that are presumably due to the device itself and the experimental setup. Around the frequency jump, we found a state which produces a harmonic frequency comb spectrum, as shown in Figure 4b. The harmonic comb spectrum was preserved under noise level of one-tenth of the shot noise but was not preserved under the shot noise level. We could not verify whether the mode-locked state can be made more stable by tuning the parameters or we need another stabilizing effect.

In Supplementary Section 9, we show that the temporal waveform is not a short and intense pulse, but rather a frequency-modulated waveform. We expect this oscillatory state corresponds to the passive mode-locked state in the experiment.

To investigate the mechanism of passive mode-locking, we performed a simulation experiment removing the nonlinear effects one by one from the conditions of Figure 4b. When we removed the feedback term with a time delay of 19.7 ps and 178 ps, we obtained neither a frequency jump nor a comb spectrum. When we replaced the nonlinear capacitance with a constant capacitance of 8 fF, we obtained a frequency jump around 303 GHz, but no comb spectrum. On the other hand, we obtained a comb spectrum when we removed the noise. Hence, feedback with a short delay time and a nonlinear capacitance are necessary for passive mode-locking, whereas noise is not necessary. As far as we know, the mode-locking caused by such effects is different from the conventional mode-locking mechanisms. It is a subject for future work to determine how these effects cause mode-locking.

Discussion

Among some previous studies on the optical feedback effect in RTD oscillator, this study is the first report of the mode-locking. There are studies showing that optical feedback affects the oscillation frequency and emission power, but their report was limited to single-mode oscillation [30][35]. There is another report implying self-pulsation due to optical feedback [36]. However, the conditions to obtain the self-pulsation and the mode-locking state have not been clarified. Pulsed emission can be obtained from RTD relaxation oscillators [37]. Although, its spectrum consists of several phase-locked modes, it is simply due to the harmonic generation.

Finally, we discuss the improvement in comb performance of the mode-locked RTD oscillator. Through hybrid mode-locking, the repetition frequency can be tuned with an external signal. Therefore, if we can stabilize the carrier-envelope offset frequency, we can obtain a fully stabilized comb spectrum. To stabilize the offset frequency, a resonant-tunneling-diode oscillator combined with a varactor diode [38] would be effective. In this oscillator, a phase-locked-loop (PLL) control through the varactor diode can be used to decrease the linewidth to less than 1 Hz in a CW oscillation state. Stabilization of one of the comb lines through PLL control would stabilize the offset frequency. Fixing one of the comb lines to a molecular absorption line will also result in narrow frequency comb lines with known absolute frequencies.

The simulation model shows that we can broaden the spectral bandwidth of the frequency comb in a different feedback condition. Figure 4c shows a simulated harmonic frequency-comb spectrum with a larger feedback amplitude. In this case, the comb spectrum is broader than in Figure 4b. The simulation showed that various broadband comb spectra can be generated depending on the feedback conditions (see Supplementary Section 10). Optimization of the feedback conditions and circuit parameters will enable us to control the bandwidth and mode spacing of the comb. It also showed the possibility to make a compact feedback configuration; optical feedback from surfaces with distances of 2.95 and 26.7 mm can cause the mode-locking even without the feedback from the mirror (see Figure S10b).

In conclusion, we clarified that a terahertz frequency comb can be obtained from a passive mode-locked resonant-tunneling-diode oscillator. Mode-locking is achieved with controlled optical feedback. We succeeded in stabilizing the repetition frequency with an additional bias-voltage modulation. The mode-locked waveform was not a short and intense pulse but rather a frequency-modulated waveform. By including the nonlinear capacitance of RTD and multiple optical feedback, a simulation model reproduced several behaviors of mode-locking. It suggested the possibility of broadband comb generation and compact feedback configuration. A better understanding of the mechanism and engineering will lead to high-performance terahertz frequency-comb generation from an RTD oscillator. Since the mode-locked RTD oscillator is based on a compact, efficient, and room-temperature operating semiconductor device, we believe it is suitable as a frequency standard for terahertz sensing and communications.

Methods

Experimental setup

A detailed schematic figure of the experimental setup is shown in Supplementary Section 1. The evaluated RTD oscillator is a prototype oscillator with a plastic leaded chip carrier package $4 \times 4 \times 2.44$ mm in size, made by Rohm Co., Ltd [23]. It was connected to a source meter and a signal generator via a bias-Tee. The RTD oscillator was biased with a DC voltage. When we wanted to show the effect of the bias modulation, we used a signal generator (RF002, RFnetworks Corporation). The signal generator was stabilized using the 10 MHz frequency reference from the atomic clocks in global positioning satellites (GPS). The current-voltage curve of the oscillator is shown in Supplementary Section 8 (1).The emission power was typically about 10 μW.

The measurement part is basically the same as that used in our previous study [39]. The local oscillator (LO) signal was a frequency-stabilized CW terahertz wave. We utilized a LO signal with a linewidth less than 240 mHz to evaluate the linewidth of the heterodyne spectrum and measure the temporal heterodyne waveform. The power of the LO signal was about 10 μW. The mixed terahertz wave was detected by a Fermi-level managed barrier diode (FMBD) with an amplifier bandwidth of 10 GHz [40]. The RF spectrum of the detected signal was measured with a spectrum analyzer (MXA 9020B, Keysight Technologies Inc). It had a bandwidth of 23 GHz and maximum resolution bandwidth of 1 Hz. The spectrum analyzer was referenced to the 10-MHz frequency reference from GPS atomic clocks. The temporal waveform of the RF signal was also measured with an oscilloscope (MSO68B 10 GHz, Tektronix Inc). It had a sampling rate of 50 GS/s and a bandwidth of 10 GHz.

We should note that there would be some inaccuracy in the measured amplitude. The sensitivity of the measurement system might have some frequency dependence because of standing waves forming [41] between the oscillator and the detector. In addition, the mixed terahertz wave was so strong that saturation of the integrated amplifier in the FMBD module [40] might have taken place. Hence, it is difficult to compare the intensity of the frequency-comb spectrum and the inter-mode beat note. It is also difficult to discuss the depth of the amplitude modulation in the temporal waveform of the passive mode-locked state.

Spectrum characterization

In the evaluation of the comb lines, we derived the frequencies of the comb lines f_n^{RF} (n = 0 to 9) as the center frequencies obtained by fitting the peaks with a Gaussian function. We fitted f_n^{RF} with equation (2), taking the linewidths of the peaks as the standard deviation of f_n^{RF}.

Similarly, in the evaluation of the inter-mode beat notes, the frequencies of the three peaks, $f_{\mathrm{IMB},m}$, were derived from a Gaussian fitting. We fitted $f_{\mathrm{IMB},m}$ with

$$f_{\mathrm{IMB},m} = m f_{\mathrm{rep}} \quad (5)$$

where m=1, 2, and 3, taking the linewidths of the peaks as the standard deviation of $f_{\mathrm{IMB},m}$. The resulting f_{rep}, 1093.16 ± 0.33 MHz, matches the value derived from the comb spectrum.

Acknowledgements

The authors would like to thank M. Asada and S. Suzuki in Tokyo Institute of Technology for valuable discussions. We appreciate Y. Takida and H. Minamide in RIKEN for their helpful discussions. This work was supported by JST ACCEL (Grant No. JPMJMI17F2).

Author Contributions

T.H. conceived the experiment, performed the measurements and analyzed the data with input from T.A. and K.T. Y.I. performed the simulation with input from T.H. and K.T. H.I. provided the Fermi-level-managed barrier diode. T.H. wrote the first draft of the manuscript and all authors contributed to manuscript revision. All work was performed under the supervision of K. T.

Competing Interests statement

The authors declare no competing financial interests.

Data Availability

The datasets generated during and/or analyzed during the current study are available from the corresponding author on reasonable request.

References

[1] Fortier, T. & Baumann, E. 20 years of developments in optical frequency comb technology and applications. *Communications Physics* **2**, 1–16 (2019)

[2] Mittleman, D. M., Jacobsen, R. H., Neelamani, R., Baraniuk, R. G. & Nuss, M. C. Gas sensing using terahertz time-domain spectroscopy. *Appl. Phys. B* **67**, 379–390 (1998)

[3] Petrov, V., Pyattaev, A., Moltchanov, D. & Koucheryavy, Y. Terahertz band communications: Applications, research challenges, and standardization activities. in *2016 8th International Congress on Ultra Modern Telecommunications and Control Systems and Workshops (ICUMT)* 183–190 (ieeexplore.ieee.org, 2016).

[4] Yasui, T., Kabetani, Y., Saneyoshi, E., Yokoyama, S. & Araki, T. Terahertz frequency comb by multifrequency-heterodyning photoconductive detection for high-accuracy, high-resolution terahertz spectroscopy. *Appl. Phys. Lett.* **88**, 241104 (2006)

[5] Faist, J. *et al.* Quantum cascade laser. *Science* **264**, 553–556 (1994)

[6] Köhler, R. *et al.* Terahertz semiconductor-heterostructure laser. *Nature* **417**, 156–159 (2002)

[7] Brandstetter, M. *et al.* High power terahertz quantum cascade lasers with symmetric wafer bonded active regions. *Appl. Phys. Lett.* **103**, 171113 (2013)

[8] Burghoff, D. *et al.* Terahertz laser frequency combs. *Nat. Photonics* **8**, 462–467 (2014)

[9] Rösch, M., Scalari, G., Beck, M. & Faist, J. Octave-spanning semiconductor laser. *Nat. Photonics* **9**, 42–47 (2014)

[10] Wienold, M., Röben, B., Schrottke, L. & Grahn, H. T. Evidence for frequency comb emission from a Fabry-Pérot terahertz quantum-cascade laser. *Opt. Express* **22**, 30410–30424 (2014)

[11] Rösch, M. *et al.* Heterogeneous terahertz quantum cascade lasers exceeding 1.9 THz spectral bandwidth and featuring dual comb operation. *Nanophotonics* **7**, 237–242 (2018)

[12] Q. Lu, F. Wang, D. Wu, S. Slivken, M. Razeghi, *Nat. Commun.* **10**, 2403 (2019).

[13] Consolino, L. *et al.* Direct Observation of Terahertz Frequency Comb Generation in Difference-Frequency Quantum Cascade Lasers. *NATO Adv. Sci. Inst. Ser. E Appl. Sci.* **11**, 1416 (2021)

[14] Wang, C., Perkins, B., Wang, Z. & Han, R. Molecular Detection for Unconcentrated Gas With ppm Sensitivity Using 220-to-320-GHz Dual-Frequency-Comb Spectrometer in CMOS. *IEEE Trans. Biomed. Circuits Syst.* **12**, 709–721 (2018)

[15] Assefzadeh, M. M. & Babakhani, A. Broadband Oscillator-Free THz Pulse Generation and Radiation Based on Direct Digital-to-Impulse Architecture. *IEEE J. Solid-State Circuits* **52**, 2905–2919 (2017)

[16] Asada, M. & Suzuki, S. Terahertz Emitter Using Resonant-Tunneling Diode and Applications. *Sensors* **21**, 1384 (2021)

[17] Brown, E. R. *et al.* Oscillations up to 712 GHz in InAs/AlSb resonant-tunneling diodes. *Appl. Phys. Lett.* **58**, 2291–2293 (1991)

[18] Feiginov, M., Sydlo, C., Cojocari, O. & Meissner, P. High-frequency nonlinear characteristics of resonant-tunnelling diodes. *Appl. Phys. Lett.* **99**, 133501 (2011)

[19] Asada, M. & Suzuki, S. Room-Temperature Oscillation of Resonant Tunneling Diodes close to 2 THz and Their Functions for Various Applications. *J. Infrared Millim. Terahertz Waves* **37**, 1185–1198 (2016).

[20] Maekawa, T., Kanaya, H., Suzuki, S. & Asada, M. Oscillation up to 1.92 THz in resonant tunneling diode by reduced conduction loss. *Appl. Phys. Express* **9**, 024101 (2016)

[21] Izumi, R., Suzuki, S. & Asada, M. 1.98 THz resonant-tunneling-diode oscillator with reduced conduction loss by thick antenna electrode. in *2017 42nd International Conference on Infrared, Millimeter, and Terahertz Waves (IRMMW-THz)* 1–2 (ieeexplore.ieee.org, 2017).

[22] Bezhko, M., Suzuki, S. & Asada, M. Frequency increase in resonant-tunneling diode cavity-type terahertz oscillator by simulation-based structure optimization. *Jpn. J. Appl. Phys.* **59**, 032004 (2020)

[23] Tsuruda, K. *et al.* Development of Practical Terahertz Packages for Resonant Tunneling Diode Oscillators and Detectors. in *2020 IEEE International Symposium on Radio-Frequency Integration Technology (RFIT)* 193–195 (ieeexplore.ieee.org, 2020).

[24] Suzuki, S., Shiraishi, M., Shibayama, H. & Asada, M. High-Power Operation of Terahertz Oscillators With Resonant Tunneling Diodes Using Impedance-Matched Antennas and Array Configuration. *IEEE J. Sel. Top. Quantum Electron.* **19**, 8500108–8500108 (2013)

[25] K. Kasagi, S. Suzuki, and M. Asada, *J. Appl. Phys.* **125**, 151601 (2019).

[26] Jaurigue, L., Nikiforov, O., Schöll, E., Breuer, S. & Lüdge, K. Dynamics of a passively mode-locked semiconductor laser subject to dual-cavity optical feedback. *Phys Rev E* **93**, 022205 (2016)

[27] Mansuripur, T. S. *et al.* Single-mode instability in standing-wave lasers: The quantum cascade laser as a self-pumped parametric oscillator. *Phys. Rev. A* **94**, 063807 (2016)

[28] Khurgin, J. B., Dikmelik, Y., Hugi, A. & Faist, J. Coherent frequency combs produced by self frequency modulation in quantum cascade lasers. *Appl. Phys. Lett.* **104**, 081118 (2014)

[29] Xue, X. *et al.* Mode-locked dark pulse Kerr combs in normal-dispersion microresonators. *Nat. Photonics* **9**, 594–600 (2015)

[30] M. Asada, S. Suzuki, Theoretical analysis of external feedback effect on oscillation characteristics of resonant-tunneling-diode terahertz oscillators. *Jpn. J. Appl. Phys.* **54**, 070309 (2015).

[31] Arkhipov, R. *et al.* Hybrid Mode Locking in Semiconductor Lasers: Simulations, Analysis, and Experiments. *IEEE J. Sel. Top. Quantum Electron.* **19**, 1100208–1100208 (2013)

[32] Wei, T. & Stapleton, S. Effect of spacer layers on capacitance of resonant tunneling diodes. *J. Appl. Phys.* **76**, 1287–1290 (1994)

[33] Asada, M., Suzuki, S. & Kishimoto, N. Resonant Tunneling Diodes for Sub-Terahertz and Terahertz Oscillators. *Japanese Journal of Applied Physics* **47** 4375–4384 (2008)

[34] Qingmin Liu, Seabaugh, A., Chahal, P. & Morris, F. J. Unified AC model for the resonant tunneling diode. *IEEE Trans. Electron Devices* **51**, 653–657 (2004)

[35] Manh, L. D. *et al.* External feedback effect in terahertz resonant tunneling diode oscillators. *IEEE Transactions on Terahertz Science and Technology* **8**, 455–464 (2018)

[36] Dal Bosco, A. K., Suzuki, S., Asada, M. & Minamide, H. Feedback Effects and Nonlinear Dynamics in Resonant Tunneling Diodes. in *2018 43rd International Conference on Infrared, Millimeter, and Terahertz Waves (IRMMW-THz)* 1–2 (2018).

[37] Verghese, S., Parker, C. D. & Brown, E. R. Phase noise of a resonant-tunneling relaxation oscillator. *Appl. Phys. Lett.* **72**, 2550–2552 (1998)

[38] Ogino, K., Suzuki, S. & Asada, M. Spectral Narrowing of a Varactor-Integrated Resonant-Tunneling-Diode Terahertz Oscillator by Phase-Locked Loop. *J. Infrared Millim. Terahertz Waves* **38**, 1477–1486 (2017)

[39] Hiraoka, T. *et al.* Injection locking and noise reduction of resonant tunneling diode terahertz oscillator. *APL Photonics* **6**, 021301 (2021)

[40] Ito, H. & Ishibashi, T. Low-noise heterodyne detection of terahertz waves at room temperature using zero-biased Fermi-level managed barrier diode. *Electron. Lett.* **54**, 1080–1082 (2018)

[41] Nahata, A., Yardley, J. T. & Heinz, T. F. Free-space electro-optic detection of continuous-wave terahertz radiation. *Appl. Phys. Lett.* **75**, 2524–2526 (1999)

Figures and Legends

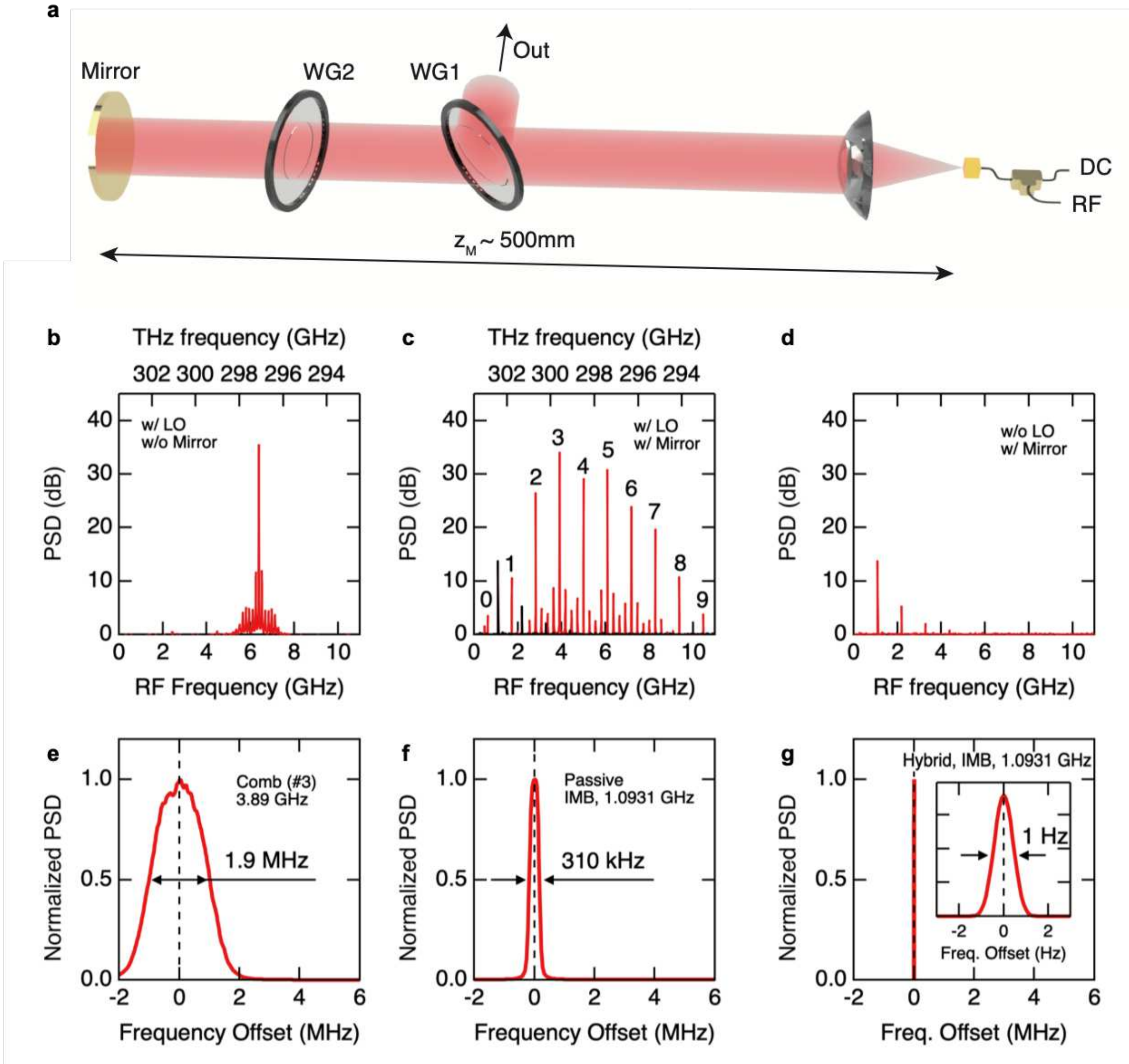

Fig. 1 THz frequency comb generation in RTD oscillator. a, Schematic diagram of the experimental setup. The RTD oscillator is biased with a DC bias voltage and generates a terahertz wave. We applied an external modulation only when we demonstrated hybrid mode-locking. The terahertz emission is split into two beams by the wire-grid polarizer WG1 with a power ratio of 1:1. The beam transmitted by WG1 is reflected at the mirror and fed back to the RTD oscillator. The distance between the mirror and the oscillator, z_{M}, is about 500 mm. It is tunable with a motorized stage on which the mirror is

mounted. The amplitude of the return light is controlled by rotating another wire-grid polarizer, WG2. WG2 is tilted to the beam in order to prevent a direct reflection to the oscillator. The beam reflected at WG1 enters the measurement part. **b**, Emission spectrum of CW oscillation state observed when the return light was blocked. The left axis shows the power spectral density (PSD) relative to the noise level. The bottom axis shows the heterodyne frequency, and the top axis shows the corresponding terahertz frequency. **c**, Frequency-comb spectrum measured with the local oscillator (LO) signal. The peaks shown by the black trace were observed even without the LO signal. The numbers at the peaks are the mode indices of the frequency comb. **d**, Emission spectrum of the passive mode-locked state measured without the LO signal. Three peaks are inter-mode beat notes. **e**, Magnified view of a comb line indexed as $n = 3$. The vertical axis is PSD normalized with the peak height. **f**, Magnified spectrum of the inter-mode beat note indexed as $m = 1$. **g**, Magnified spectrum of the inter-mode beat note indexed as $m = 1$ when the bias modulation was applied (Hybrid mode-locked state). These spectra were accumulated over 1 second. The bias voltage was 471 mV.

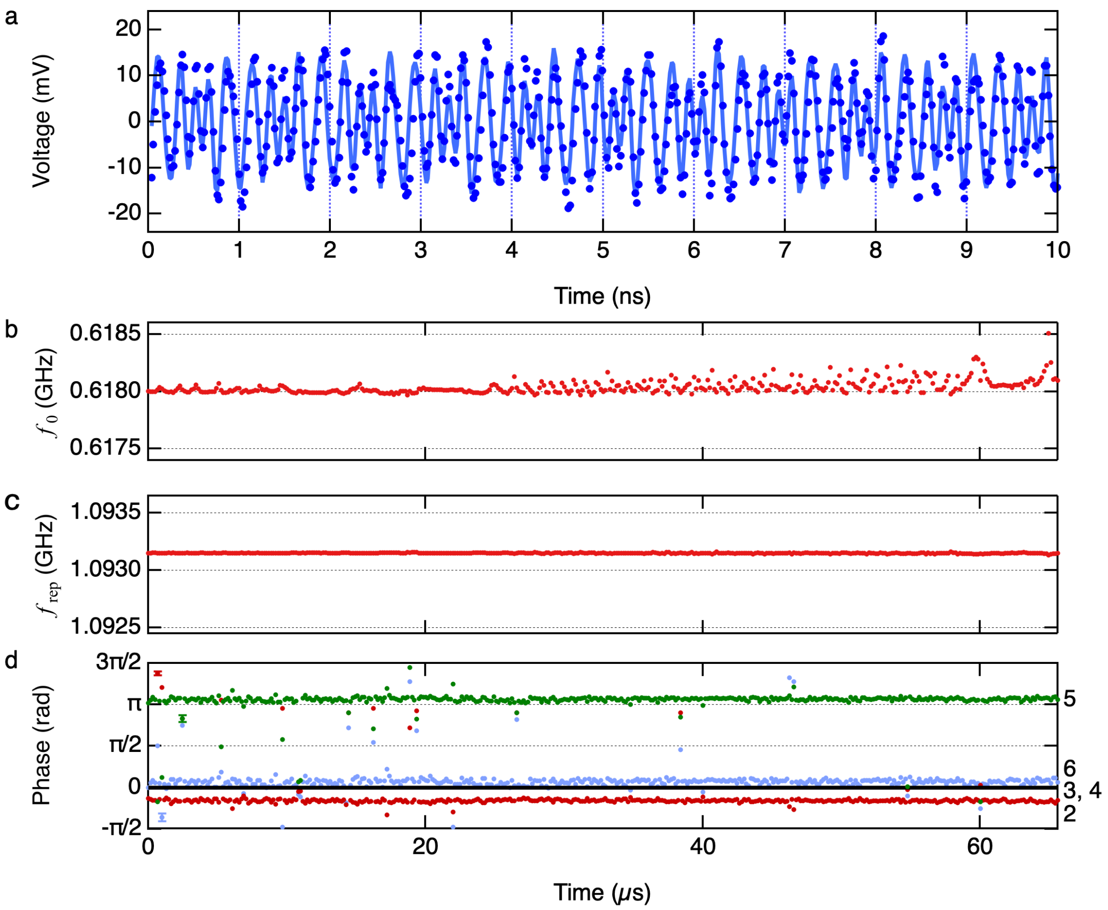

Fig. 2 Fixed relationship between modal phases. a, Measured heterodyne temporal waveform of passive mode-locked state (dots) and fitting curve (trace) plotted over 10 ns. The temporal resolution of the measurement was 20 ps. Long-term stability of **b**, offset frequency, **c**, repetition frequency, and **d**, relative initial phases over 65.6 μs. The numbers beside the right axis show the mode indices corresponding to the markers. The error bars show the estimated standard deviation of the fitting parameter. In Figures 2b and 2c, the error bars are smaller than the marker size. In Figure 2d, the error bars are shown in one data point in the first few μs for each marker as a typical value.

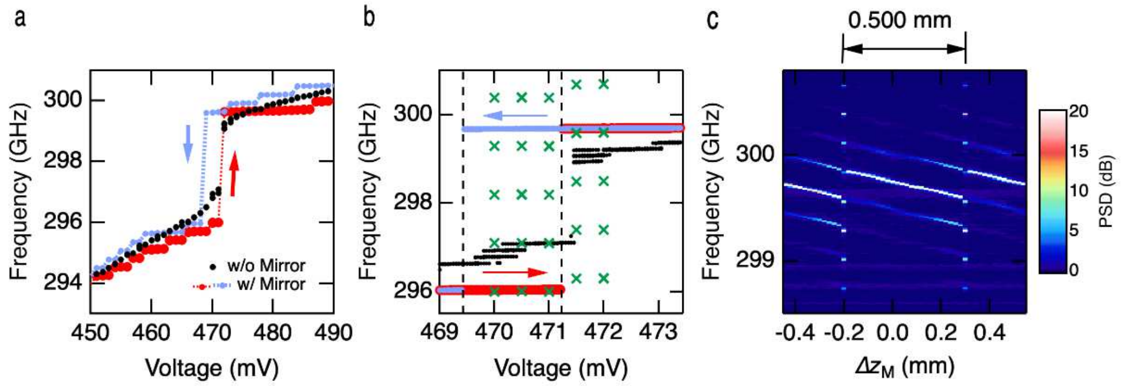

Fig. 3 Conditions of passive mode-locking. a, Frequency-voltage curve measured without mirror (black dots), with mirror and up-swept voltage (red dots), and with mirror and down-swept voltage (blue dots). Significant hysteresis on the sweep direction was not observed in the case of no mirror. **b**, Frequency-voltage curve measured around the frequency jump point (markers are the same as in **a**). The green crosses show the frequencies of the comb peaks observed when the mirror was swept at each bias voltage. **c**, THz spectrum observed when the mirror was swept with a bias voltage of 471 mV. The horizontal axis shows the shift of the mirror position Δz_{M}. The sweep direction was the one in which Δz_{M} decreases. These figures were measured with the maximum feedback amplitude in our setup. The frequency resolution was 11 MHz. The data points in Figure 3a and 3b were extracted from the series of spectra obtained during the voltage sweep and are the frequency points that had a PSD larger than the noise level by 20 dB.

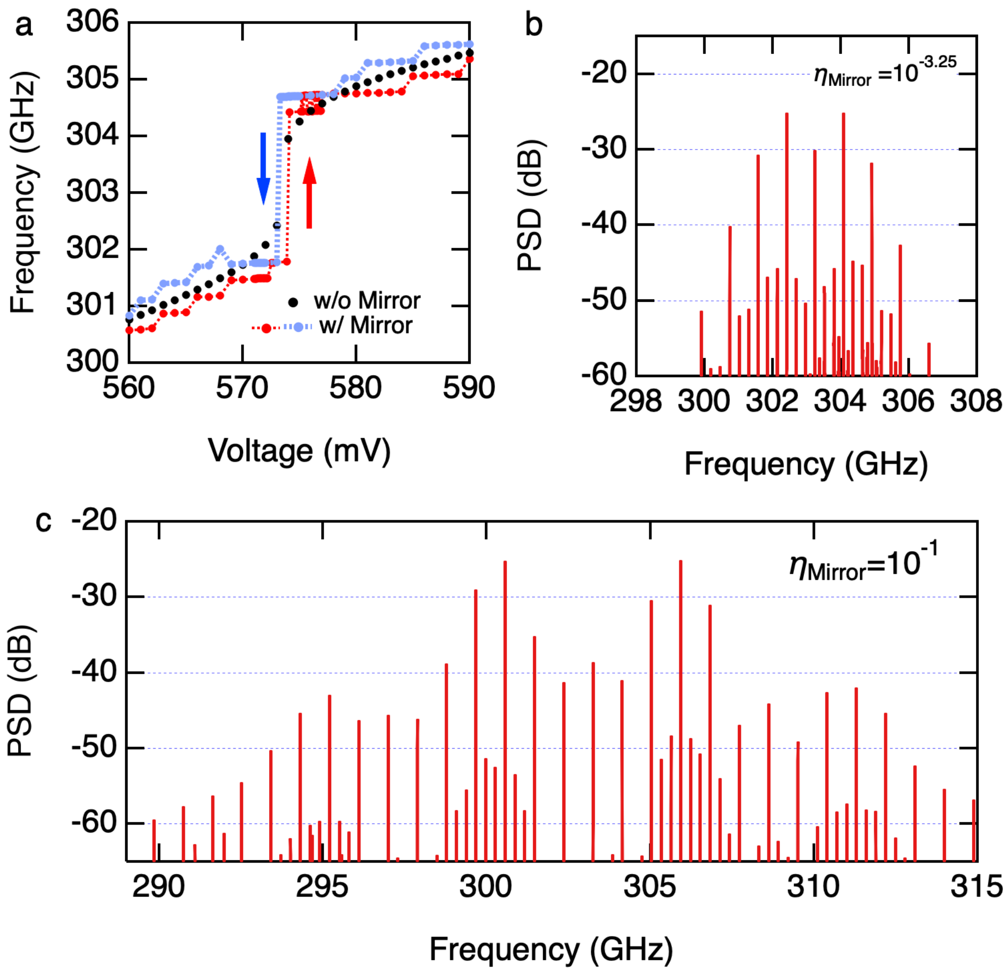

Fig. 4 Circuit simulation. a, Wide-range frequency-voltage characteristics. In the simulation, the temporal waveform was calculated by sweeping the bias voltage. At each data point, the voltage sweep was stopped, and the temporal waveform was simulated for 0.62 μs. The spectrum was obtained by Fourier transforming the temporal waveform of the last 0.1 μs. The shot noise described in Supplementary Section 8 (1) was included. **b**, Harmonic frequency comb spectrum simulated for reflectivity $\eta_{\mathrm{Mirror}} = 10^{-3.25}$, which corresponds to the experimental condition. **c,** Harmonic frequency comb spectrum simulated for $\eta_{\mathrm{Mirror}} = 10^{-1}$. Since the circuit has a nonradiative loss, it

corresponds to the case where all the emitted power is fed back from the mirror. The results in Figures 4b and 4c obtained under the following conditions: the bias voltage was 573.5 mV. The temporal waveform was simulated over 11.0 µs, and the spectrum was calculated using the last 1.0 µs. Noise had a standard deviation 10 times smaller than the shot noise.

Supplementary Files

This is a list of supplementary files associated with this preprint. Click to download.

- PMLRTDSup20210919.pdf